Water Air Soil Pollut (2023) 234:390
https://doi.org/10.1007/s11270-023-06385-7

Assessing the Efficiency and Mechanism of Copper Adsorption onto Biochars derived from Corn Straw and Cow Manure

Qiao Xu · Chuanqi Xiong · Jialu Fan · Feifan Zhang · Jingjing Wang · Qiuyue Xu · Weiqin Yin · Shengsen Wang · Xiaozhi Wang

Received: 21 October 2022 / Accepted: 23 May 2023 / Published online: 10 June 2023

Abstract The adsorption efficiency and mechanism of Cu^{2+} were qualitatively and quantitatively assessed in solution by biochar pyrolyzed at 500 ℃ (CSB500 vs. CMB500) using different agricultural wastes (corn straw vs. cow manure). The adsorption kinetic, isotherm fittings and pH effect were investigated and surface characterization was carried out before and after Cu^{2+} adsorption. The Langmuir isotherm was the best fit for both biochars and CMB500 had a higher maximum Cu^{2+} adsorption capacity (78.63 mg g^{-1}) than CSB500 (73.77 mg g^{-1}). The adsorption capacity reached the largest at pH 6.0 with 21.24 mg g^{-1} for CSB500 and 24.28 mg g^{-1} for CMB500. The adsorption mechanisms for Cu^{2+} adsorption were different for the two biochars. Specifically, cation exchange and mineral precipitation contributed 43.5% and 33.2% for Cu^{2+} adsorption by CSB500 respectively. The most important mechanism for CMB500 is mineral precipitation and the contribution is 60.7%, probably due to the high mineral components of CMB500 which are easily precipitated with Cu^{2+}. The correlation analysis illustrated that total Cu^{2+} removal capacity is highly positively correlated with mineral precipitation, pH, ash content, specific surface area and total P of biochar. The results benefit for selection of highly efficient biochar materials based on their physicochemical properties for better Cu^{2+} removal from wastewaters.

Keywords Biochar · Copper · Adsorption characteristics · Adsorption mechanism

Supplementary Information The online version contains supplementary material available at https://doi.org/10.1007/s11270-023-06385-7.

Q. Xu · C. Xiong · J. Fan · F. Zhang · J. Wang · Q. Xu · W. Yin · S. Wang · X. Wang
College of Environmental Science and Engineering, Yangzhou University, Yangzhou 225127, Jiangsu, China

Q. Xu
Key Laboratory of Arable Land Quality Monitoring and Evaluation, Ministry of Agriculture and Rural Affairs, Yangzhou University, Yangzhou 225127, China

X. Wang (✉)
Joint International Research Laboratory of Agriculture and Agri-Product Safety of Ministry of Education of China, Yangzhou University, Yangzhou 225127, Jiangsu, China
e-mail: xzwang@yzu.edu.cn

1 Introduction

As non-degradable contaminants, heavy metals are metallic elements with a high density, which have invoked severe environmental damage and health problems for living organisms via bioaccumulation and biomagnification (Demirbas, 2008). As a common heavy metal, copper (Cu) is also an essential mineral nutrient for human health and nutrition, however, excess exposure to copper can cause cellular damage and disease (Xie et al., 2017).

To remediate heavy metal pollutants in the environment, various methods and technologies have been explored and generalized as membrane separation (Shariful et al., 2018), ion exchange (Cavaco et al., 2007), chemical precipitation (Meunier et al., 2006) and adsorption (Toles & Marshall, 2002). Among these, adsorption is easy to handle and a cost-effective approach (Demirbas, 2008). Common adsorbents are activated carbon, resin, municipal sludge, agricultural waste etc., but these adsorbents are of their disadvantages due to either low efficiency, high cost, lack of source and/or potential secondary pollution (Jia et al., 2008). Therefore, it is particularly important to produce low-cost and environment-friendly adsorption materials.

Biochar produced from anaerobic pyrolysis of biomass is considered to be a new type of environmental functional material, the effect of which in remediation of heavy metal-contaminated wastewater has been widely evaluated (Ahmad et al., 2014a, b; Beesley et al., 2015; Xu et al., 2022). Various biomass can be used in the production of biochar, including animal manure (Batool et al., 2017; Xu et al., 2013), herbaceous plants (Hwang et al., 2013), agricultural by-products, and municipal sludges (Chagas et al., 2021; Fan et al., 2020), etc. The physical and chemical properties of biochar mainly depend on the characteristics of feedstock and the pyrolysis temperature, which would thus affect the adsorption efficiency and capacity. Generally, under the same preparation conditions, the ash content and pH of biochar prepared from animal manure and sludge are higher than those prepared from herbs and agricultural by-products, while the biochar derived from herbs has higher carbon content and lower cation exchange capacity (CEC) than that derived from animal manure (Ahmad et al., 2014a, b; Uchimiya et al., 2010; Yaman, 2004). High ash content, large specific surface area, and abundant functional groups have been reported as the main characteristics of biochar with higher heavy metal removal capacity.

Biochars produced from different feedstocks show significantly different Cu^{2+} removal capacities in solution. For example, the maximum adsorption capacity of manure-derived biochars for Cu^{2+} is 39.79 mg g^{-1}–43.59 mg g^{-1} (308 k) (Batool et al., 2017), while the sludge-derived biochars showed a quite low maximum adsorption capacity for Cu^{2+}, which was 0.96 mg g^{-1}–2.46 mg g^{-1} (Fan et al., 2020). The maximum adsorption capacity for Cu^{2+} by willow biochar and cow dung biochar is 12.2 mg g^{-1} and 14.7 mg g^{-1}, respectively (Wang et al., 2020). The main mechanisms of heavy metal adsorption by biochar include: 1) mineral precipitation, 2) complexation of heavy metals with oxygen-containing functional groups, 3) cation-π interaction and 4) the exchange of heavy metal ions with positively charged ions such as K^+, Ca^{2+}, Na^+, and Mg^{2+} (Gao et al., 2019; Trakal et al., 2014). Studies are still inadequate regarding systematic comparison of the capacities of biochars pyrolyzed from different feedstocks in Cu^{2+} adsorption. Moreover, mechanisms that regulate Cu^{2+} adsorption may differ among biochars and the relative contribution of adsorption mechanisms warrant further research to better discern, produce and/or modify biochar with high heavy metal (e.g. Cu) remediation capacity.

The study aims to systematically examine the adsorption characteristics of Cu^{2+} by biochar prepared from two common raw materials (corn straw and cow manure) with different characteristics and to qualitatively compare the contribution of each mechanism to total Cu^{2+} adsorption by the biochars. Besides, this study further related the adsorption mechanism with biochar physicochemical properties by correlation analysis. We hypothesized that: 1) cow manure biochar has greater Cu^{2+} adsorption capacity due to its high ash content and CEC; 2) the relative contribution of adsorption mechanisms is different for manure and plant litter-derived biochars.

2 Materials and Methods

2.1 Biochar Preparation and Characterization

Corn straw and cow manure were chosen as biochar feedstocks and pyrolyzed under an atmosphere of nitrogen gas at 500 ℃. Briefly, the feedstocks were firstly chopped into small pieces before packing them into quartz pyrolysis tubes. Both ends of the pyrolysis tubes were then sealed with stainless steel sealing flanges. Nitrogen gas was injected at a flow rate of 500 ml min^{-1} for 30 min to form an oxygen-limiting environment inside the pyrolysis tubes. The pyrolysis temperature was gradually raised to 500 ℃ with a heating rate of 5 ℃ min^{-1} and maintained for 2 h. After pyrolysis, the biochars were cooled down

to room temperature by circulating nitrogen gas. The corn straw- and cow manure-derived biochars were ground to pass a 60-mesh sieve and named CSB500 and CMB500, respectively.

The yield of biochar was calculated from the mass loss of the corn straw and cow manure before and after pyrolysis. The pH and EC of biochar were measured according to the standard method of IBI (2015). The ash content of biochar was determined by ashfying the biochar in a muffle furnace at 800 ℃ for 4 h and weighing the biomass left. The cation exchange capacity of biochar was determined by the sodium acetate exchange method (Gaskin et al., 2008). The total phosphorus (P) and potassium (K) in biochar were determined after digestion with sulfuric acid and hydrogen peroxide.

The specific surface area (SSA) of biochar was determined by an ASAP 2460 analyzer (ASAP2460, Micromeritics, USA). The contents of C, H, O and N in biochar were determined by an elemental analyzer (ELIII, Elementar Vario, Germany). The microstructure of biochar was characterized by scanning electron microscopy (S-4800II, Hitachi, Japan). Reactive functional groups of biochar were determined via a micro infrared spectrometer (Cary 610/670, Agilent, USA). X-ray diffraction (XRD) patterns of biochar before and after Cu^{2+} adsorption were acquired by an X-Ray diffractometer (Ultima IV, Rigaku Corporation, Japan) with diffraction angles between 2–80°. An X-Ray photoelectron spectroscopy (ESCALAB 250Xi, Thermo, USA) was used to discern the elemental oxidation states and functional groups of the original biochar materials.

2.2 Batch Adsorption Experiment

To evaluate the effect of feedstock type on adsorption efficiency of Cu^{2+} by biochar, batch adsorption experiments were conducted under the following conditions: 20.0 mg biochar was mixed with 20 mL Cu^{2+} stock solution (25–150 mg L^{-1}) at different pH (3.0–6.0) and then agitated for different time (5–1440 min) at 185 rpm (Cui et al., 2016; Deng et al., 2018; Wang et al., 2018). All experiments were carried out in triplicates at 25 ℃. The suspension was sampled at the given time and filtered through a 0.45 μm filter membrane for Cu^{2+} determination using a flame atomic absorption spectrophotometer (PinAAcle 900F, PerkinElmer, Singapore). The loaded Cu^{2+} onto biochar materials was collected and oven-dried after experiment and disposed as hazardous waste.

2.2.1 *Factors Affecting Cu^{2+} Adsorption*

To examine the process parameter on adsorption efficiency of Cu^{2+}, various pH gradients (3.0, 4.0, 5.0 and 6.0) and contact time (5 min, 10 min, 20 min, 30 min, 1 h, 2 h, 4 h, 6 h, 10 h and 24 h) were set up with the initial concentration of $CuSO_4$ solution being 25 mg $Cu{\cdot}L^{-1}$ and the suspension pH being adjusted to the specific pH with diluted HCl and NaOH. All other conditions were kept the same as described above. The pseudo-first-order and second-order kinetic equations were used to describe the kinetic process of Cu^{2+} adsorption on biochar. The equations are as follows:

$$q_t = q_e(1 - e^{-k_1 t}) \tag{1}$$

$$q_t = \frac{k_2 q_e^2 t}{1 + k_2 q_e t} \tag{2}$$

In which, 't' is the adsorption time, h; 'q_t' is the adsorption capacity of Cu^{2+} on biochar at time t, mg g^{-1}; 'q_e' is the adsorption capacity at equilibrium, $mg{\cdot}g^{-1}$; 'k_1' (h^{-1}) and 'k_2' ($g{\cdot}mg^{-1}\ h^{-1}$) are the pseudo-first-order and second-order kinetic constants, respectively.

2.2.2 *Adsorption Isotherm*

Adsorption isotherm was adopted to examine the relationship between the quantity of Cu^{2+} adsorbed by biochar and the total quantity of Cu^{2+} in solution. Briefly, 20 mg biochar was mixed with 20 mL $CuSO_4$ solution made with 0.01 mol L^{-1} $NaNO_3$ solution, with a Cu^{2+} concentration of 25, 50, 75, 100 and 150 mg L^{-1}. The experiment was conducted in triplicate with the initial pH being adjusted to 5.0 with diluted HCl and NaOH. The suspension was oscillated at 25 ℃ for 24 h and then filtered through 0.45 μm for Cu^{2+} determination. The Freundlich and Langmuir isothermal adsorption models were used to fit the adsorption data of Cu^{2+} by biochar using the following equations:

$$lnq_e = lnK_f + \frac{1}{n} lnc_e \quad (3)$$

$$\frac{c_e}{q_e} = \frac{1}{b \times q_m} + \frac{C_e}{q_m} \quad (4)$$

Where 'c_e' is the equilibrium adsorption concentration of Cu^{2+}, $mg \cdot L^{-1}$; 'q_e' and 'q_m' are the equilibrium adsorption capacity and the maximum adsorption capacity, $mg \cdot g^{-1}$; 'K_f' is the adsorption capacity parameter, $mg \cdot g^{-1}$; 'n' is the Freundlich constant, indicating the adsorption strength; parameter 'b' ($L \cdot mg^{-1}$) characterizes the adsorption site affinity for metals on the adsorbent surface.

2.3 Contribution of Different Adsorption Mechanisms

The mechanisms for Cu^{2+} adsorption on the surface of biochar were precipitation, cation exchange, complexation with oxygen-containing functional groups and coordination with π-electrons. The relative contribution of which to total Cu^{2+} adsorption was partitioned according to (O'Connor et al., 2022).

The adsorption capacity by mineral precipitation (Q_{cp}) was obtained from the difference in adsorption capacity of demineralized and untreated biochar using the following equation:

$$Q_{cp} = Q_t - Q_a \quad (5)$$

Where 'Q_t' is the total adsorption capacity; 'Q_a' is the adsorption capacity by demineralized biochar. The biochar was demineralized by acid washing using 1 mol L^{-1} HCl and rinsing with deionized water till constant pH.

The adsorption capacity generated by cation exchange (Q_{ci}) was obtained from the release of K^+, Ca^{2+}, Na^+ and Mg^{2+} before and after adsorption by biochar using the following equation:

$$Q_{ci} = Q_K + Q_{Ca} + Q_{Na} + Q_{Mg} \quad (6)$$

In which, 'Q_K', 'Q_{Ca}', 'Q_{Na}' and 'Q_{Mg}' are the amount of K^+, Ca^{2+}, Na^+ and Mg^{2+} released into solution by biochar after adsorption.

The adsorption capacity obtained by complexation with oxygen-containing functional groups (Q_{cf}) was determined by changes in solution pH (H^+ concentration) after and before Cu^{2+} adsorption by the demineralized biochar and calculated with the following equation:

$$Q_{cf} = 1000 \times (10^{-pH_A} - 10^{-pH_B}) \quad (7)$$

In the formula, pH_A and pH_B represent the pH values of the solution after (A) and before (B) adsorption of Cu^{2+} by demineralized biochar.

Other adsorption mechanisms (Q_{co}) i.e., the coordination of Cu^{2+} with π-electrons was calculated using the following equation:

$$Q_{co} = Q_t - Q_{ci} - Q_{cf} \quad (8)$$

Where 'Q_t' is the total adsorption capacity of Cu^{2+} on biochar.

2.4 Statistical Analysis

Descriptive statistics were conducted using the SPSS statistical 19.0 program (IBM SPSS, Inc, Chicago, USA). Model fitting of adsorption kinetics and isotherms and the correlation heatmap were generated using Origin 2019 (OriginLab Corp., Northampton, USA). XRD analysis of mineral types was performed using jade 5.0 (MDI, Newtown Square, USA) with the 2004 card libraries.

3 Results and Discussion

3.1 Biochar Characterization

The adsorbent performance of heavy metal by biochar is regulated by biochar properties (e.g. ash content, mineral and carbon content, specific surface area and aromaticity etc.) which differ intrinsically with feedstock type under the same pyrolysis process. Raw materials undergo different degrees of dehydration, branched chain breaking and recombination, aromatic condensation, and other processes in the pyrolysis process. Cow manure contained higher amounts of minerals which are involatile during pyrolysis and thus remained in the biochar, leading to the higher yield and ash content in CMB500 when compared to CSB500 (Table 1), which may result in differences in the adsorption mechanisms of the two biochars for metals. The alkalinity of biochar is determined mainly by the ash content (Yuan et al., 2011; Zheng et al., 2013) and thus the pH of CMB500 was slightly

Table 1 Basal characteristics of corn straw biochar (CSB500) and cow manure biochar (CMB500)

Biochar		CSB500	CMB500
Ash content (%)		21.75 ± 0.11	35.55 ± 0.25
Yield		31.57 ± 0.13	47.16 ± 0.14
pH		10.58 ± 0.01	10.71 ± 0.13
EC ($ms \cdot cm^{-1}$)		2.71 ± 0.03	0.27 ± 0.00
CEC ($cmol.kg^{-1}$)		55.96 ± 2.17	98.87 ± 1.78
BET ($m^2 \cdot g^{-1}$)		21.06 ± 0.08	31.41 ± 0.06
Total K		79.99 ± 0.78	31.54 ± 0.57
Total P		8.87 ± 0.77	13.52 ± 0.09
Elemental content(%)	**C**	61.96	51.22
	H	2.81	2.48
	O	11.43	8.58
	N	1.60	1.82
	S	0.45	0.35

higher than that of CSB500 (Table 1). The morphology of both biochars were analyzed by SEM and the porous surface structures of both biochars suggested great potential to adsorb Cu^{2+} ion. Specifically, CSB500 had a strip structure with a clear pore structure and obvious tube bundle structure on the surface (Fig. 1a, b) and CMB500 had a tubular structure with abundant pores (Fig. 1c, d), which rendered it with a larger specific surface area (Table 1). From the results of elemental analysis, CSB500 had higher carbon content but lower H/C than CMB500 (Table 1), indicating CSB500 had a more stable aromatic and π-conjugated structure than CMB500. CSB500 also had slightly higher O content, O/C ratio and (O + N)/C ratio than CMB500, suggesting CSB500 contained more oxygen-containing functional groups.

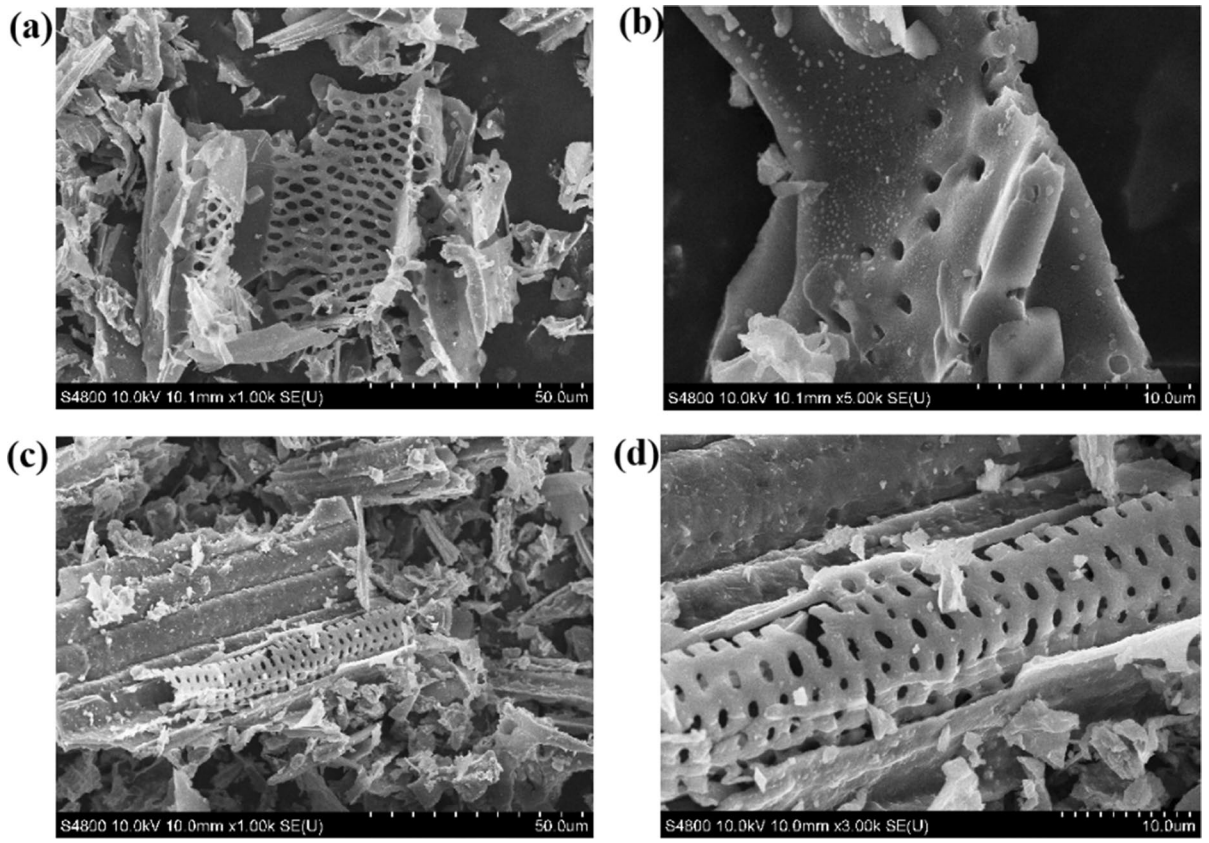

Fig. 1 SEM images of corn straw biochar (CSB500, **a**, **b**) and cow manure biochar (CMB500, **c**, **d**)

3.2 Cu^{2+} Adsorption Kinetics and Isotherms

The adsorption reaction is driven by the interaction between adsorbents and sorbates, with the surface adsorption and desorption balance being regulated by factors such as contact time, the concentration of metal ions and pH (Li & Xie, 2003). The adsorption sites of both biochars reached saturation quickly (~24 h) after reaction with Cu^{2+} as shown by the kinetic curves (Fig. 2a) due to greater numbers of reactive groups. The pseudo-second-order model performed better to characterize the adsorption pattern of Cu^{2+} onto biochars than the pseudo-first-order model based on the higher adjusted coefficient of determination (R^2) and smaller difference between the theoretical adsorption equilibrium (Q_e) and the measured value (Fig. 2a, Table S1). The CMB500 had slightly higher Cu^{2+} adsorption capacity but longer equilibrium time when compared to CSB500 (Fig. 2a), probably due to its higher specific surface area, pore volumes and binging energy with Cu^{2+}.

How biochars as adsorbates interact with Cu^{2+} is further featured by isotherm adsorption. The adsorption isotherm at different initial Cu^{2+} content on the two biochars was shown in Fig. 2b. The Langmuir and Freundlich isotherm models were applied and the corresponding fitting parameters were given in Table S2. The Langmuir isotherm describes adsorption on identical surfaces with irrelevant cooperation between the adsorbed particles and accepts that the adsorption and desorption are relative to the accessible surface and the involved surface, individually (Li et al., 2017). The Freundlich isotherm model expects that the outer

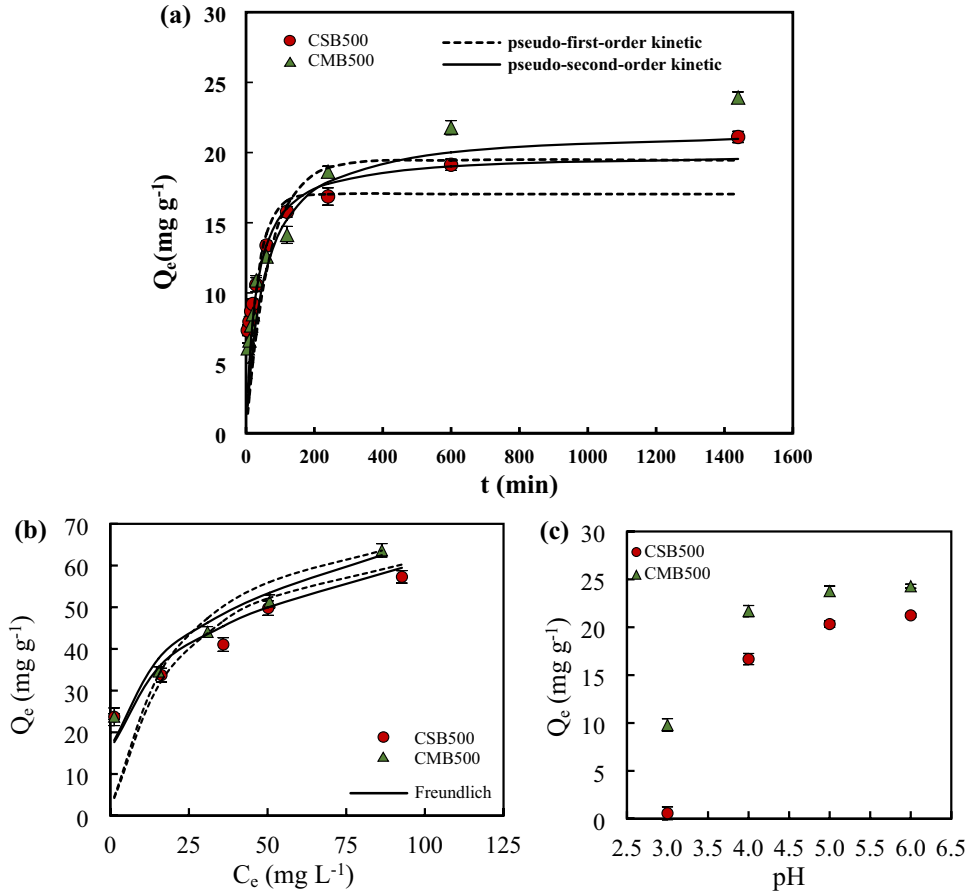

Fig. 2 Fitting of the adsorption of Cu^{2+} kinetic data to the pseudo-first-order and second-order models (**a**), Freundlich and Langmuir isotherm fittings for the adsorption of Cu^{2+} (**b**) and the effect of pH on Cu^{2+} adsorption (**c**) by corn straw biochar (CSB500) and cow manure biochar (CMB500)

layer of the adsorbate is heterogenous with various affinities to the adsorbent and that adsorption happens in a multi-facet design (O'Connor et al., 2022). The Cu^{2+} adsorption isotherm by CSB500 and CMB500 could be better fitted using the Freundlich model (Table S2). The maximum adsorption capacity increased with initial Cu^{2+} ion concentration and obtained from the Langmuir model was 78.63 mg g^{-1} and 73.77 mg g^{-1} for CMB500 and CSB500, respectively. The results are higher than a series of reports using different adsorbents for Cu^{2+} removal in solution. For example, the maximum Cu^{2+} sorption was determined as 44.50 mg g^{-1} and 43.68 mg g^{-1} for a farmyard, manure- and poultry manure-derived biochar respectively (Batool et al., 2017). However, other factors (e.g. pyrolysis temperature, application rate) may also regulate the Cu^{2+} adsorption by biochar and should be focused on in further studies.

3.3 Effect of pH on Cu^{2+} Adsorption

The pH value of the solution is an important environmental factor affecting the adsorption efficiency of heavy metal ions. pH can not only affect the functional groups on the surface of biochar but also change the existing form of metal ions in the solution (Milmile et al., 2011). The biochars showed low capacities in adsorbing Cu^{2+} at a pH lower than 3.0 (Fig. 3c). The amount of Cu^{2+} removed by biochars increased significantly with the increase in pH from 3.0 to 6.0. However, the adsorption capacity leveled out when the solution pH was greater than 6.0. The CMB500 had greater Cu^{2+} adsorption capacity than CSB500 regardless of solution pH. The mechanisms of absorbent behavior as affected by pH are summarized as follows. Firstly, the positive charges on the surface of the biochar at low pH are repulsive to Cu^{2+} in the solution (Wang et al., 2018), which is unfavorable to the adsorption of Cu^{2+} (Fig. S1). Secondly,

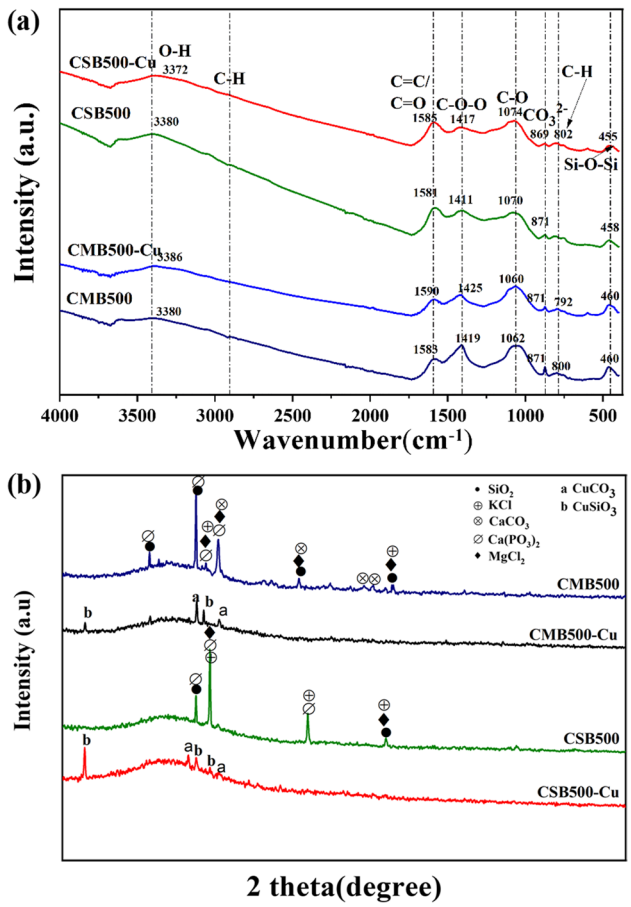

Fig. 3 FT-IR spectra (**a**) and XRD diffractograms (**b**) of corn straw biochar (CSB500) and cow manure biochar (CMB500) before and after adsorption of Cu^{2+}

biochar releases more cations (K^+, Ca^{2+}, Mg^{2+}, etc.) and anions (CO_3^{2-}, PO_4^{3-}, SO_4^{2-}, etc.) from previously insoluble crystal minerals in the low pH environment (Fig. 3b). The cations might compete with Cu^{2+} for active adsorption sites on biochar surface and the anions are difficult to precipitate with Cu^{2+} at low pH (Liu et al., 2019; Qiu et al., 2008). Moreover, as solution pH rises, the content of H^+ decreases, while the negative surface charge of biochar increases (Sánchez-Polo & Rivera-Utrilla, 2002), which favors the electrostatic interaction with Cu^{2+}, thus promoting the adsorption of Cu^{2+} by biochar. When the solution pH is greater than 6.0, Cu^{2+} will precipitate to form $Cu(OH)^+$, $Cu(OH)_2^{2+}$, $Cu_3(OH)_4^{2+}$, and the content of soluble Cu^{2+} decreases in the solution (Fig. S1), thus affecting the adsorption efficiency. Therefore, a pH of 5.0 was suggested as the optimum pH for the Cu^{2+} adsorption experiment in this study.

3.4 Mechanisms of Cu^{2+} Adsorption on Biochars

3.4.1 Ion Exchange

Cations in biochar, including K^+, Na^+, Ca^{2+}, Mg^{2+} etc., remain in biochar through electrostatic attraction, precipitation, and complexation with functional groups (e.g. carboxyl groups), and these ions can be replaced by the adsorption process between biochar and heavy metals (Ahmed et al., 2016; Cui et al., 2016), which was confirmed by this study as the concentrations of K^+, Na^+, Ca^{2+}, and Mg^{2+} in the solution increased after Cu^{2+} adsorption. Therefore, cation exchange is a possible mechanism for Cu^{2+} adsorption by biochar (Bernardo et al., 2013).

3.4.2 Mineral Precipitation

Previous studies have shown that Cu^{2+} can form precipitation with some anions released from biochar into aqueous solution, such as CO_3^{2-}, PO_4^{3-} and OH^- (Chi et al., 2017; Deng et al., 2018; Shen et al., 2017). To qualitatively analyze the role of precipitation in the process of Cu^{2+} adsorption by biochar, the X-ray diffraction patterns of the two biochars before and after Cu^{2+} adsorption were determined (Fig. 3b). The biochars before Cu^{2+} adsorption had more abundant characteristic peaks and higher mineral contents. After Cu^{2+} adsorption, both biochars showed $CuSiO_3$ generation at $2\theta = 12.80°$ and 26.68°, and $CuCO_3$ generation at $2\theta = 25.72°$. Besides, CSB500 also showed $CuSiO_3$ generation at $2\theta = 28.39°$, while CMB500 also showed $CuCO_3$ generation at $2\theta = 29.45°$.

The infrared characterization spectra of the two biochars before and after Cu^{2+} adsorption was present in Fig. 3a. The corresponding peak at 458 cm^{-1} is the Si-O-Si vibration absorption peak (Babu et al., 2011), and the corresponding peak at 871 cm^{-1} is CO_3^{2-} vibration absorption peak. (Reig et al., 2002). Compared with the original biochar, the intensity of these bands changed after Cu^{2+} adsorption, indicating the formation of silicon complexes or silicon mineral precipitation and phosphate precipitation in the process of Cu^{2+} adsorption. The XRD results were consistent with FT-IR, indicating that mineral precipitation is one of the mechanisms of Cu^{2+} adsorption by biochar (Xu et al., 2013).

3.4.3 Complexation of Oxygen-Containing Functional Groups

FT-IR was used to characterize the changes in oxygen-containing functional groups on the surface of biochar before and after Cu^{2+} adsorption (Fig. 3a). The corresponding bands at 3380 cm^{-1} are O-H vibration absorption peaks of the hydroxyl group, the corresponding peaks at 1411 cm^{-1} (CSB500) and 1419 cm^{-1} (CMB500) are C-O-O (Yang et al., 2007), and the corresponding peaks at 1070 cm^{-1} (CSB500) and 1062 cm^{-1} (CMB500) are C-O. The strength and position of these bands changed after Cu^{2+} adsorption, suggesting that there was complexation with oxygen-containing functional groups in the process of Cu^{2+} adsorption. Generally, the complexation process of -COOH and -OH functional groups with Cu^{2+} is accompanied by the release of H^+ (Cao et al., 2009), which leads to a decrease in the solution pH (Fig. S2). C1s spectra were deconvoluted into four major components at binding energies of 289.6/289.0 eV, 286.3/285.8 eV, 284.7/285.0 eV and 284.4 eV, which were signalized by O–C=O, C=O, C–O and C–C, respectively (Fig. S3) and the concentration of C–C, C=O and O–C=O is higher for CMB500 than CSB500. The oxygen-containing functional groups in biochar provided abundant adsorption sites for Cu^{2+} adsorption, and the contribution of this mechanism to total adsorption capacity will be discussed later.

3.4.4 Other Mechanisms

In addition to the above mechanisms, other possible heavy metal adsorption mechanisms, such as physical adsorption, π-coordination, and electrostatic attraction, have also been proposed in the modified biochar (Yuan et al., 2020; Zhu et al., 2020). Biochar is highly aromatic and rich in aromatic π structure, therefore it can be used as an electron-π carrier to combine with heavy metals. Previous studies have shown that the surface of biochar prepared at a high temperature can form strong metal-π ligand with heavy metals (Swiatkowski et al., 2004). According to FT-IR spectrum analysis, the corresponding peak at 792 cm^{-1} was aromatic C-H bending vibration (Huang et al., 2017; Xu et al., 2013), and the corresponding peak at 1581 cm^{-1} (CSB500) and 1583 cm^{-1} (CSB500) was aromatic C=C stretching vibration, and the intensity of these bands changed because of Cu^{2+} adsorption. These heterocyclic compounds are weak cation-π bonds, which can easily combine with Cu^{2+} by providing π-electrons (Keiluweit & Kleber, 2009). The results referred that there is cation-π interaction in the process of Cu^{2+} adsorption by biochar (Uchimiya et al., 2010).

3.5 Contribution of Adsorption Mechanisms and the Correlation with Biochar Properties

The main adsorption mechanism of Cu^{2+} on the two biochars were summarized in Fig. 4 as: (I) surface complexation of Cu^{2+} with oxygen-containing functional groups, Q_{cf}; (II) ion exchange, Q_{ci}; (III) co-precipitation of Cu^{2+} with mineral components, Q_{cp} and (IV) other potential mechanisms, Q_{co} (cation-π interaction between Cu^{2+} and π electron of aromatic structure (C=C), electrostatic interaction, etc.). Most of the minerals in the biochar were removed after acid pickling, however, the oxygen-containing functional groups of the biochar did not change before and after acid pickling. Therefore, the reduction of the adsorption capacity of the biochar after demineralization is regarded as the contribution of minerals to the total adsorption (Qiu et al., 2008).

Ion exchange and mineral precipitation were the dominating mechanisms for CSB500 in adsorbing Cu^{2+} and their contributions were quantified at 43.5% and 33.2%, respectively (Fig. 4a). The contribution of mineral precipitation was 60.7%, rendering it the most important mechanism of Cu^{2+} adsorption by CMB500 probably due to the high mineral components of CMB500 which easily precipitated with Cu^{2+}. Besides, ion exchange was the second most important contributor (28.5%) for Cu^{2+} adsorption by CMB500. The correlation analysis showed that the total adsorption capacity (Q_t) was positively correlated with Q_{cp}, pH, ash content, CEC and total P (Fig. 5), indicating the mineral composition of biochar plays a very important role in the adsorption of Cu^{2+}. The high pH value of biochar is conducive to the de-protonation of oxygen-containing functional groups, so that all biochars

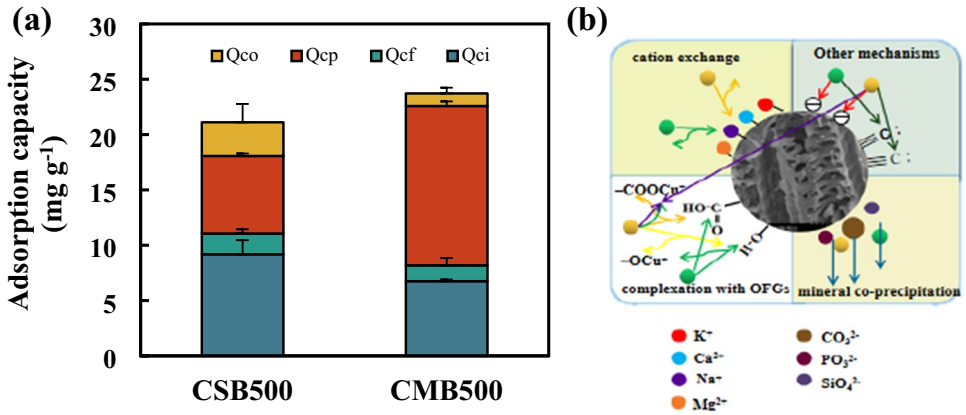

Fig. 4 Contribution of mineral precipitation (Q_{cp}), cation exchange (Q_{ci}), complexation with oxygen-containing functional groups (Q_{cf}) and coordination with π-electrons (Q_{co}) to the adsorption of Cu^{2+} (**a**) by corn straw biochar (CSB500) and cow manure biochar (CMB500) and the mechanism diagram of Cu^{2+} adsorption by biochar (**b**)

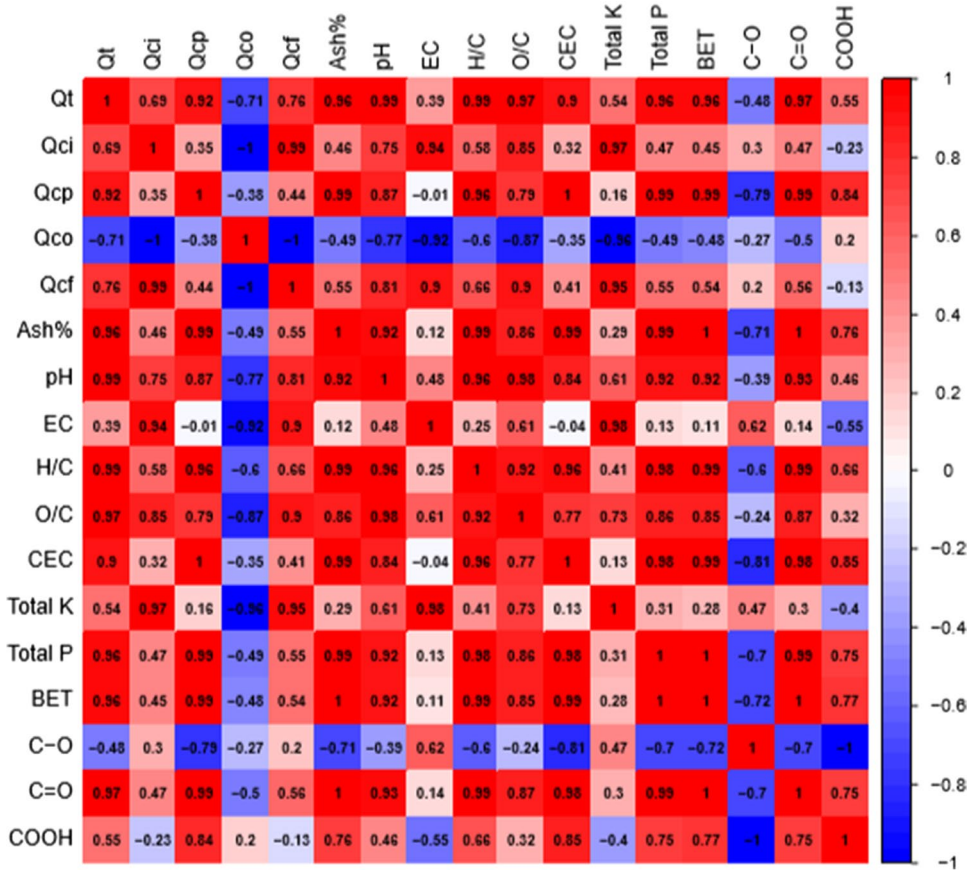

Fig. 5 Correlation heatmap of Cu^{2+} adsorption mechanisms (Q_{cp}, mineral precipitation; Q_{ex}, cationic exchange; Q_{cf}, complexation with oxygen-containing functional groups and Q_{co}, coordination with π-electrons) with biochar characteristics. Q_t, total Cu^{2+} adsorption capacity

surfaces will produce negative adsorption sites, which are beneficial for the adsorption of Cu^{2+}. The positive correlation between Q_{ci} and EC and total K indicates that Cu^{2+} interacts with soluble minerals containing potassium. Q_{cp} was highly positively correlated with ash content, CEC, and total P content, indicating that the formation of Cu-phosphate precipitation possibly because PO_4^{3-} released by biochar contributed to the immobilization of Cu^{2+}, which is confirmed by the weakening of peak strength of calcium phosphate in the XRD pattern after adsorption. There was a high positive correlation between Q_{cf} and O/C, confirming that the content of oxygen-containing functional groups would affect the adsorption effect of Cu^{2+}.

4 Conclusion

The animal manure-derived biochar (CMB500) has a slightly higher Cu^{2+} removal capacity than the corn straw-derived biochar (CSB500). Mineral precipitation and cation exchange are the most two important mechanisms for Cu^{2+} adsorption and their relative contributions are different for the two biochars. Specifically, the contribution of mineral precipitation is 60.7% and 28.5%, cation exchange is 33.2% and 43.5% for CMB500 and CSB500, respectively. Total Cu^{2+} removal capacity is highly positively correlated with mineral precipitation, pH, ash content, specific surface area and total P of biochar from the correlation analysis. The results help in select highly efficient biochar materials based on their physicochemical

properties and surface characterization for better Cu^{2+} removal from wastewaters.

Author Contributions Xu, Q.: Conceptualization, Writing- Original draft preparation, Writing- Reviewing, Editing. Fan, J.L., Xiong, C.Q., Zhang, F.F., Wang J.J. and Xu, Q.Y.: Methodology, Investigation, Writing- Original draft preparation. Yin, W.Q.: Investigation, Conceptualization, Methodology. Wang, S.S.: Methodology, Writing- Reviewing and Editing. Wang X.Z.: Funding acquisition, Writing- Reviewing and Editing, Supervision. All authors have participated in the preparation of this manuscript and have approved the final version.

Funding This work is supported by National Natural Science Foundation of China (grant number 41977085, 42007075, 31772394), China Scholarship Council, the National Key Research and Development Program of China (2021YFD1700800), the 333 Project in Jiangsu Province (BRA2020300) and Six-talent peaks project in Jiangsu Province (TD-JNHB-012).

Data Availability All data generated or analyzed during this study are included in this published article.

Declarations

Competing Interests The authors declare no competing interests.

References

Ahmad, M., Moon, D. H., Vithanage, M., Koutsospyros, A., Lee, S. S., Yang, J. E., Lee, S. E., Jeon, C., & Ok, Y. S. (2014). Production and use of biochar from buffalo-weed (Ambrosia trifida L.) for trichloroethylene removal from water. *Journal of Chemical Technology and Biotechnology, 89*(1), 150–157.

Ahmad, M., Rajapaksha, A. U., Lim, J. E., Zhang, M., Bolan, N., Mohan, D., Vithanage, M., Lee, S. S., & Ok, Y. S. (2014b). Biochar as a sorbent for contaminant management in soil and water: A review. *Chemosphere, 99*, 19–33.

Ahmed, M. B., Zhou, J. L., Ngo, H. H., Guo, W., & Chen, M. (2016). Progress in the preparation and application of modified biochar for improved contaminant removal from water and wastewater. *Bioresource Technology, 214*, 836–851.

Babu, B. C., Naresh, V., Prakash, B. J., & Buddhudu, S. (2011). Structural, thermal and dielectric properties of lithium zinc silicate ceramic powders by sol-gel method. *Ferroelectrics Letters Section, 38*(4–6), 114–127.

Batool, S., Idrees, M., Hussain, Q., & Kong, J. (2017). Adsorption of copper (II) by using derived-farmyard and poultry manure biochars: Efficiency and mechanism. *Chemical Physics Letters, 689*, 190–198.

Beesley, L., Moreno-Jimenez, E., Fellet, G., Melo, L., Sizmur, T. (2015). Biochar and heavy metals. In J. Lehmann and S. Joesph (Eds.), Biochar for Environmental Management (2nd ed., pp. 595–626). Routledge.

Bernardo, M., Mendes, S., Lapa, N., Gonçalves, M., Mendes, B., Pinto, F., Lopes, H., & Fonseca, I. (2013). Removal of lead (Pb^{2+}) from aqueous medium by using chars from co-pyrolysis. *Journal of Colloid and Interface Science, 409*, 158–165.

Cao, X., Ma, L., Gao, B., & Harris, W. (2009). Dairy-manure derived biochar effectively sorbs lead and atrazine. *Environmental Science and Technology, 43*(9), 3285–3291.

Cavaco, S. A., Fernandes, S., Quina, M. M., & Ferreira, L. M. (2007). Removal of chromium from electroplating industry effluents by ion exchange resins. *Journal of Hazardous Materials, 144*(3), 634–638.

Chagas, J., Figueiredo, C. C., de Silva, J. D., Shah, K., & Paz-Ferreiro, J. (2021). Long-term effects of sewage sludge–derived biochar on the accumulation and availability of trace elements in a tropical soil. *Journal of Environmental Quality, 50*(1), 264–277.

Chi, T., Zuo, J., & Liu, F. (2017). Performance and mechanism for cadmium and lead adsorption from water and soil by corn straw biochar. *Frontiers of Environmental Science and Engineering, 11*(2), 1–8.

Cui, X., Fang, S., Yao, Y., Li, T., Ni, Q., Yang, X., & He, Z. (2016). Potential mechanisms of cadmium removal from aqueous solution by *Canna indica* derived biochar. *Science of the Total Environment, 562*, 517–525.

Demirbas, A. (2008). Heavy metal adsorption onto agro-based waste materials: A review. *Journal of Hazardous Materials, 157*(2–3), 220–229.

Deng, Y., Huang, S., Laird, D. A., Wang, X., & Dong, C. (2018). Quantitative mechanisms of cadmium adsorption on rice straw- and swine manure-derived biochars. *Environmental Science and Pollution Research, 25*(32), 32418–32432.

Fan, J., Li, Y., Yu, H., Li, Y., Yuan, Q., Xiao, H., Li, F., & Pan, B. (2020). Using sewage sludge with high ash content for biochar production and Cu(II) sorption. *Science of the Total Environment, 713*, 136663.

Gao, L. Y., Deng, J. H., Huang, G. F., Li, K., Cai, K. Z., Liu, Y., & Huang, F. (2019). Relative distribution of Cd^{2+} adsorption mechanisms on biochars derived from rice straw and sewage sludge. *Bioresource Technology, 272*, 114–122.

Gaskin, J. W., Steiner, C., Harris, K., Das, K. C., & Bibens, B. (2008). Effect of low-temperature pyrolysis conditions on biochar for agricultural use. *Transactions of the ASABE, 51*(6), 2061–2069.

Huang, H., Tang, J., Gao, K., He, R., Zhao, H., & Werner, D. (2017). Characterization of KOH modified biochars from different pyrolysis temperatures and enhanced adsorption of antibiotics. *RSC Advances, 7*(24), 14640–14648.

Hwang, H., Oh, S., Cho, T. S., Choi, I. G., & Choi, J. W. (2013). Fast pyrolysis of potassium impregnated poplar wood and characterization of its influence on the formation as well as properties of pyrolytic products. *Bioresource Technology, 150*, 359–366.

IBI (2015). Standardized Product Definition and Product Testing Guidelines for Biochar that Is Used in Soil,

International Biochar Initiative. http://www.biochar-international.org/characterizationstandard

Jia, D. A., Zhou, D. M., Wang, Y. J., Zhu, H. W., & Chen, J. L. (2008). Adsorption and cosorption of Cu(II) and tetracycline on two soils with different characteristics. *Geoderma, 146*(1–2), 224–230.

Keiluweit, M., & Kleber, M. (2009). Molecular-level interactions in soils and sediments: The role of aromatic pi-systems. *Environmental Science and Technology, 43*(10), 3421–3429.

Li, H., Dong, X., da Silva, E. B., de Oliveira, L. M., Chen, Y., & Ma, L. Q. (2017). Mechanisms of metal sorption by biochars: Biochar characteristics and modifications. *Chemosphere, 178*, 466–478.

Li, X., Xie, G. (2003). Characteristics and effecting factors of adsorption time of coalbed gas reservoir. *Natural Gas Geoscience*, 502–505.

Liu, L., Huang, Y., Zhang, S., Gong, Y., Su, Y., Cao, J., & Hu, H. (2019). Adsorption characteristics and mechanism of Pb(II) by agricultural waste-derived biochars produced from a pilot-scale pyrolysis system. *Waste Management, 100*, 287–295.

Meunier, N., Drogui, P., Montané, C., Hausler, R., Mercier, G., & Blais, J. F. (2006). Comparison between electrocoagulation and chemical precipitation for metals removal from acidic soil leachate. *Journal of Hazardous Materials, 137*(1), 581–590.

Milmile, S. N., Pande, J. V., Karmakar, S., Bansiwal, A., Chakrabarti, T., & Biniwale, R. B. (2011). Equilibrium isotherm and kinetic modeling of the adsorption of nitrates by anion exchange Indion NSSR resin. *Desalination, 276*(1–3), 38–44.

O'Connor, K. F., Al-Abed, S. R., Hordern, S., & Pinto, P. X. (2022). Assessing the efficiency and mechanism of zinc adsorption onto biochars from poultry litter and softwood feedstocks. *Bioresource Technology Reports, 18*, 101039.

Qiu, Y., Cheng, H., Xu, C., & Sheng, G. D. (2008). Surface characteristics of crop-residue-derived black carbon and lead(II) adsorption. *Water Research, 42*(3), 567–574.

Reig, F., Gimeno-Adelantado, J. V., & Moreno, M. (2002). FTIR Quantitative Analysis of Calcium Carbonate (Calcite) and Silica (Quartz) Mixtures Using the Constant Ratio Method. Application to Geological Samples. *Talanta, 58*, 811–821.

Sánchez-Polo, M., & Rivera-Utrilla, J. (2002). Adsorbent-adsorbate interactions in the adsorption of Cd(II) and Hg(II) on ozonized activated carbons. *Environmental Science and Technology, 36*(17), 3850–3854.

Shariful, M. I., Sepehr, T., Mehrali, M., Ang, B. C., & Amalina, M. A. (2018). Adsorption capability of heavy metals by chitosan/poly(ethylene oxide)/activated carbon electrospun nanofibrous membrane. *Journal of Applied Polymer Science, 135*(7), 45851.

Shen, Z., Zhang, Y., McMillan, O., Jin, F., & Al-Tabbaa, A. (2017). Characteristics and mechanisms of nickel adsorption on biochars produced from wheat straw pellets and rice husk. *Environmental Science and Pollution Research, 24*(14), 12809–12819.

Swiatkowski, A., Pakula, M., Biniak, S., & Walczyk, M. (2004). Influence of the surface chemistry of modified activated carbon on its electrochemical behaviour in the presence of lead(II) ions. *Carbon, 42*(15), 3057–3069.

Toles, C. A., & Marshall, W. E. (2002). Copper ion removal by almond shell carbons and commercial carbons: Batch and column studies. *Separation Science and Technology, 37*(10), 2369–2383.

Trakal, L., Bingöl, D., Pohořelý, M., Hruška, M., & Komárek, M. (2014). Geochemical and spectroscopic investigations of Cd and Pb sorption mechanisms on contrasting biochars: Engineering implications. *Bioresource Technology, 171*, 442–451.

Uchimiya, M., Lima, I. M., Thomas Klasson, K., Chang, S., Wartelle, L. H., & Rodgers, J. E. (2010). Immobilization of heavy metal ions (CuII, CdII, NiII, and PbII) by broiler litter-derived biochars in water and soil. *Journal of Agricultural and Food Chemistry, 58*(9), 5538–5544.

Wang, R. Z., Huang, D. L., Liu, Y. G., Zhang, C., Lai, C., Zeng, G. M., Cheng, M., Gong, X. M., Wan, J., & Luo, H. (2018). Investigating the adsorption behavior and the relative distribution of Cd^{2+} sorption mechanisms on biochars by different feedstock. *Bioresource Technology, 261*, 265–271.

Wang, S., Kwak, J. H., Islam, M. S., Naeth, M. A., Gamal El-Din, M., & Chang, S. X. (2020). Biochar surface complexation and Ni(II), Cu(II), and Cd(II) adsorption in aqueous solutions depend on feedstock type. *Science of the Total Environment, 712*, 136538.

Xie, R., Jin, Y., Chen, Y., & Jiang, W. (2017). The importance of surface functional groups in the adsorption of copper onto walnut shell derived activated carbon. *Water Science and Technology, 76*(11), 3022–3034.

Xu, X., Cao, X., Zhao, L., Wang, H., Yu, H., & Gao, B. (2013). Removal of Cu, Zn, and Cd from aqueous solutions by the dairy manure-derived biochar. *Environmental Science and Pollution Research, 20*(1), 358–368.

Xu, Q., Xu, Q. Y., Zhu, H., Li, H., Yin, W. Q., Feng, K., Wang, S. S., & Wang, X. Z. (2022). Does biochar application in heavy metal-contaminated soils affect soil micronutrient dynamics? *Chemosphere, 290*, 133349.

Yaman, S. (2004). Pyrolysis of biomass to produce fuels and chemical feedstocks. *Energy Conversion and Management, 45*(5), 651–671.

Yang, H., Yan, R., Chen, H., Lee, D. H., & Zheng, C. (2007). Characteristics of hemicellulose, cellulose and lignin pyrolysis. *Fuel, 86*(12–13), 1781–1788.

Yuan, J. H., Xu, R. K., & Zhang, H. (2011). The forms of alkalis in the biochar produced from crop residues at different temperatures. *Bioresource Technology, 102*(3), 3488–3497.

Yuan, S., Hong, M., Li, H., Ye, Z., Gong, H., Zhang, J., Huang, Q., & Tan, Z. (2020). Contributions and mechanisms of components in modified biochar to adsorb cadmium in aqueous solution. *Science of the Total Environment, 733*, 139320.

Zheng, H., Wang, Z., Deng, X., Zhao, J., Luo, Y., Novak, J., Herbert, S., & Xing, B. (2013). Characteristics and nutrient values of biochars produced from giant reed at different temperatures. *Bioresource Technology, 130*, 463–471.

Zhu, L., Tong, L., Zhao, N., Wang, X., Yang, X., & Lv, Y. (2020). Key factors and microscopic mechanisms

controlling adsorption of cadmium by surface oxidized and aminated biochars. *Journal of Hazardous Materials, 382*, 121002.